

Supporting Information

Wächter et al. 10.1073/pnas.1011581108

SI Text

True and Apparent Stiffness, Correction for Limited Video Frequency.

Magnetic beads (typical radius 0.5 μm). Thermal fluctuations, if recorded by video at a given frame rate, are averaged over the frame duration, such that their apparent variance is less than the true one. In the context of this work, this variance leads to overestimation of the elastic stiffness of a given bead-spring construct. The following error discussion is based on chapter 4 (“Thermal Forces and Diffusion”) in ref. 1.

Rotary motion of a microscaled bead attached to a torsion spring is overdamped and its autocorrelation function decays exponentially:

$$R(t) = \frac{k_B T}{\kappa} \exp\left(-\frac{\kappa}{\gamma} t\right). \quad [\text{S1}]$$

Herein k_B denotes the Boltzmann constant, T the temperature, κ the elastic stiffness of the torsion spring, γ the viscous drag coefficient of the bead, and t the time.

The magnitude of R at time zero equals the variance, σ^2 , which is a consequence of the equipartition principle:

$$R(0) = \frac{k_B T}{\kappa} = \sigma^2 \quad [\text{S2}]$$

The so called “power spectrum” of the autocorrelation function, $G(\omega)$, its Fourier transform, reads as follows:

$$G(\omega) = 4 \int_0^\infty R(t) \cdot \cos \omega t \cdot dt = \frac{4k_B T \gamma}{\kappa^2} \cdot \frac{1}{[1 + (\frac{\omega}{\omega_0})^2]}, \quad [\text{S3}]$$

where ω denotes the angular frequency and ω_0 the “corner frequency” (or cutoff frequency) of the Lorentzian spectrum,

$$\omega_0 = \frac{\kappa}{\gamma}. \quad [\text{S4}]$$

When presented as the reverse Fourier transformation, $R(t)$ reads

$$R(t) = \frac{1}{2\pi} \int_0^\infty G(\omega) \cdot \cos \omega t \cdot d\omega \quad [\text{S5}]$$

and at time zero

$$R(0) = \frac{1}{2\pi} \int_0^\infty G(\omega) \cdot d\omega = \frac{2}{\pi} \cdot \frac{k_B T}{\kappa} \cdot \arctan \frac{\infty}{\omega_0} = \frac{k_B T}{\kappa}, \quad [\text{S6}]$$

see Eq. S2 above.

If the fluctuations are recorded by an instrument with limited time resolution, as in video recordings, fluctuations occurring at higher frequencies than the limiting frequency of the instrument are suppressed. As a consequence, the apparent variance is smaller and the apparent stiffness greater than the respective true one:

$$\begin{aligned} R_{\text{app}}(0) &= \frac{1}{2\pi} \int_0^{\omega_l} G(\omega) \cdot d\omega = \frac{2}{\pi} \cdot \frac{k_B T}{\kappa} \cdot \arctan \frac{\omega_l}{\omega_0} = \sigma_{\text{app}}^2 \\ &= \frac{k_B T}{\kappa_{\text{app}}}. \end{aligned} \quad [\text{S7}]$$

The true stiffness (κ) is smaller than the apparent stiffness (κ_{app}), and the correction factor depends on the ratio between the limiting frequency (ω_l) and the corner frequency (ω_0) of the Lorentzian (Eq. S4):

$$\kappa = \frac{\arctan \omega_l / \omega_0}{\pi/2} \cdot \kappa_{\text{app}}. \quad [\text{S8}]$$

According to the sampling theorem, the limiting frequency of a digital recording is half the sampling frequency. In the present video system, the frame rate was 25 s⁻¹. The limiting angular frequency then is

$$\omega_l = 1/2 \cdot 2\pi \cdot 25 \text{ s}^{-1}. \quad [\text{S9}]$$

The angular corner frequency (ω_0 , see Eq. S4) is difficult to assess with precision. The attachment mode of the bead to the spring (central versus off-central), variations of the bead diameter, and flow coupling between bead and surface all affect the viscous drag coefficient, γ . A centrally rotating bead ($\gamma = 8\pi\eta R^3$) moving in bulk water ($\eta_{\text{H}_2\text{O}} = 10^{-3} \text{ kgm}^{-1} \text{ s}^{-1}$) gives the lowest estimate for the drag coefficient and thus an upper limit for the corner frequency. For a bead radius of 0.5 μm,

$$\omega_0 \leq \omega_0^{(a)} = \frac{\kappa}{3.14}, \quad [\text{S10}]$$

where κ comes in piconewton nanometer.

The relation between the apparent and the true stiffness is plotted in Fig. S5 for two different viscous drag coefficients, the one of a centrally attached sphere (radius 0.5 μm) moving in bulk water, and a threefold larger drag (accounting for eccentric attachment and higher viscosity due to flow coupling).

It is obvious from Fig. S5 that video-recorded fluctuations of a bead with 0.5-μm radius yielding an apparent stiffness of up to 200 pNnm approximate the true stiffness reasonably well. An apparent stiffness of 500 pNnm may be up to twofold overrated, and the overrating increases further with growing κ_{app} .

In the context of the present work, two properties are noteworthy: (i) The order of apparent stiffness monotonously follows the order of true stiffness; in other words, differences are meaningful, whether corrected or not. (ii) An apparent stator stiffness of 1,700 pNnm implies a true stiffness of at least 500 pNnm, which is still at least 10 times more rigid than the most flexible domain on the rotor of EF₀F₁ whose corrected stiffness is 35 pNnm (see below). In other words, the conclusions of Sielaff et al. (2) and this work are valid and independent of the correction, namely, (i) F₀ and F₁ are linked by a stiff stator, and (ii) their cooperation is smoothed by an elastically compliant rotor.

Actin filaments (typical length 0.5–0.8 nm). In previous experiments aiming mainly at the stiffness of the rotor in EF₀F₁, we used actin filaments as probes and selected those single filaments that were fixed at one end to the enzyme and discarded those fixed in the middle and rotating as a propeller (2). The respective drag coefficient is

$$\gamma_{\text{fil}} = \frac{4\pi\eta L^3}{3(\ln L/r - 0.447)}, \quad [\text{S11}]$$

where η is the medium viscosity, L the length, and r the cylinder radius of the filament.

Assuming a length of $0.8 \mu\text{m}$, a radius of 2.8 nm , the viscosity as in pure water $10^{-3} \text{ kgm}^{-1} \text{ s}^{-1}$, and a true stiffness of 35 pNnm , the calculated corner frequency of the respective Lorentzian is $\omega_0 = 83 \text{ s}^{-1}$, such that the apparent stiffness is 75 pNnm as reported for EF_0F_1 with the filament attached to the c ring (bend-

ing mode of deformation) and the engineered disulfide lock between rotor and stator placed in the top of EF_1 (2). The elastically highly compliant domain between F_0 and F_1 is thus probably twofold more flexible than was previously reported.

1. Howard J (2001) *Mechanics of Motor Proteins and Cytoskeleton* (Sinauer, Sunderland, MA).

2. Sielaff H, et al. (2008) Domain compliance and elastic power transmission in rotary $\text{F}_0\text{F}_1\text{-ATPase}$. *Proc Natl Acad Sci USA* 105:17760–17765.

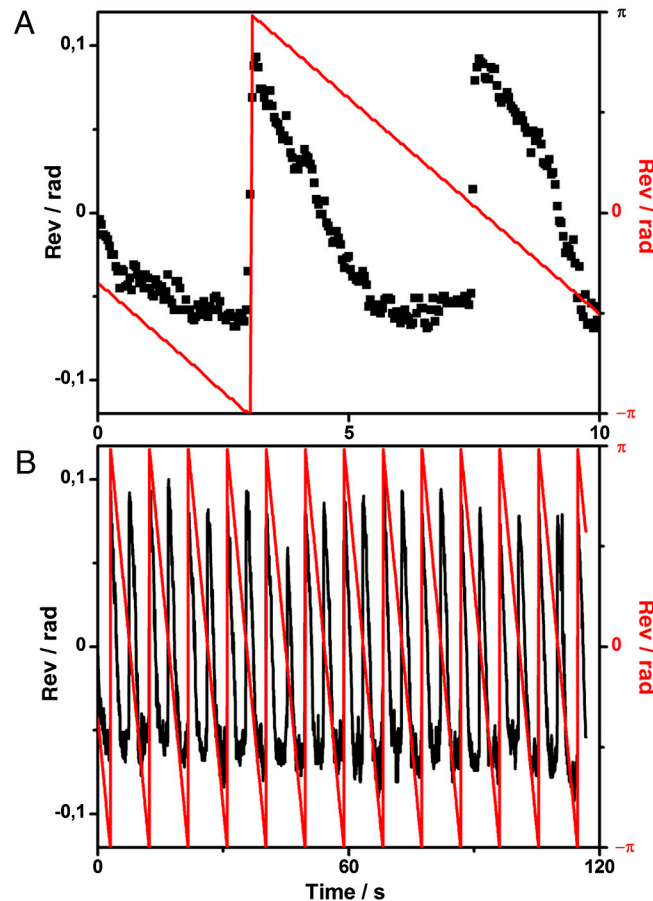


Fig. S1. Magnetorotation trajectory of the same bead- EF_0F_1 constructs as shown in Movie S1 [black; mutant SD466 (3-gly)]. Two magnets were mounted at opposite positions on a rotating disk. The rotation rate was 0.107 rev/s . The rotary trajectory of the disk between $-\pi$ and $+\pi$ is shown in red, the trajectory of the bead in black. The relaxed orientation of the bead in absence of a magnetic field is set at 0° . (A) Excerpt of first 10 s, and (B) full trajectory over 2 min. Every single frame-based bead position is shown as a quad.

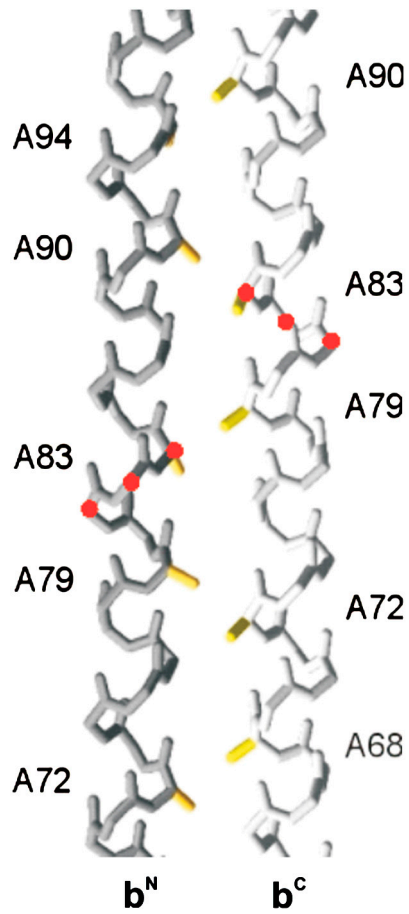


Fig. S4. Model structure of the right-handed coiled coil of b_2 that is slightly off-register. The red dots indicate the C_α atoms with glycine substitution in the mutant 3-gly.

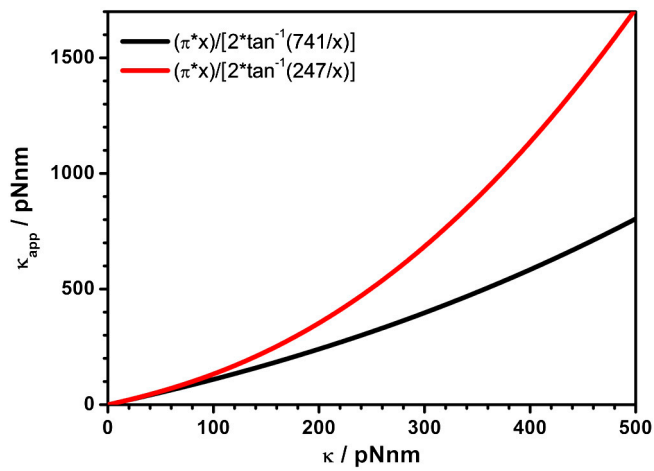


Fig. S5. Apparent versus true stiffness calculated according to Eq. S8 (see text).

